GEOLOGICA CARPATHICA, DECEMBER 2023, 74, 6, 489–500 https://doi.org/10.31577/GeolCarp.2023.28

Unravelling the tectonic phases: The impact of the South Caspian Block on Late Cenozoic deformation in the Central Alborz, Iran

FAEZEH SAFARI[1] and ALI YASSAGHI[1, ✉]

[1]Department of Geology, Tarbiat Modares University, Tehran, Iran; ✉ yassaghi@modares.ac.ir

(Manuscript received September 13, 2023; accepted in revised form January 13, 2024; Associate Editor: Rastislav Vojtko)

Abstract: Paleostress reconstruction through polyphase fault-slip data of a multi-deformed region suffered collisional tectonics can lead to detecting the stress phases. Based on earthquakes' focal mechanisms and morphotectonic features, multiple deformation phases model has been proposed for the Alborz Mountains located in the collision zone between the Arabian (Central Iran) and Eurasian (South Caspian block) plates during the Late Cenozoic. In this study, paleostress analysis has been carried out in an area bounded by two (Kandovan and Taleghan) regional faults in the Central Alborz Mountains using fault-slip data. This analysis resulted in the identification of three main tectonic phases. The first, compressional phase is proposed to cause the inversion of the Alborz Mountains' major initial normal faults to reverse faults during the convergence of the Arabian and Eurasian plates. The second, transpressional phase is offered as a factor for the reactivation of the hidden Alborz basement faults to form the NE-striking left-lateral strike-slip faults on the sedimentary cover. The third, transtensional phase is suggested to be responsible for the development of the NNE–SSW left-lateral transtensional faults. It is proposed that the second and third paleostress phases are affected mainly by the indentation of the South Caspian Block into the Alborz Mountains during the Late Cenozoic.

Keywords: South Caspian Block, Central Alborz, paleostress analysis, Late Cenozoic deformation

Introduction

The Alborz Mountains in the north of Iran (Fig. 1a) is extended for about 600 km in length and 100 km in width from the Talesh Mountains, as the southern continuation of the Caucasus Mountains in the west to the Kopet-Dagh Mountains in the east. The Alborz Mountains wrapped around the South Caspian Block (SCB) have suffered several deformation phases (Berberian 1983; Alavi 1996). It is generally believed that SCB has a critical role in the mountains' deformational complexities through its southwestward movement during the Late Cenozoic (Axen et al. 2001; Jackson et al. 2002; Allen et al. 2003a, b, 2004; Guest et al. 2006; Rashidi et al. 2023) or its northwestward movement since about 1–1.5 Ma (Ritz et al. 2006; Djamour et al. 2010). Since SCB has no seismicity and there is no GPS measurement of its activity, its movement and imposed deformation should be detected through its effect on surrounding mountains i.e., Talesh, Alborz, and Kopet-Dagh (Fig. 1a).

The central part of the Alborz Mountains comprises several regional reverse faults with right or left-lateral strike-slip minor components (e.g., Allen et al. 2003a, 2004; Ritz et al. 2006; Yassaghi & Madanipour 2008; Yassaghi & Naeimi 2011). These faults are oriented parallel to the Alborz Mountains trend and are dipping inside the mountains (Annells et al. 1975; Gansser & Hubber 1962) (Fig. 1b). Paleomagnetic data has confirmed two dominant deformation episodes across the Central Alborz (Ballato et al. 2008; Cifelli et al. 2015; Mattei et al. 2017). The first deformational stage resulted from the north-south convergence of the Arabia-Eurasia plates and affected the entire Iranian Plateau since the Neogene caused the formation of the Alborz Mountains' regional reverse faults (Axen et al. 2001; Jackson et al. 2002; Allen et al. 2003a, b, 2004; Guest 2004; Guest et al. 2006; Ballato et al. 2013). The second stage, since the late Miocene (6 Ma) caused kinematic change in the minor component of the reverse faults from right-lateral to left-lateral strike-slip component (Axen et al. 2001; Jackson et al. 2002; Allen et al. 2003a, b, 2004; Guest et al. 2006; Rashidi et al. 2023). They believe this episode has acted coeval with the southwestward movement of SCB. Other contemporaneous events such as acceleration in sedimentation rate in the Caspian Basin (Jackson et al. 2002), sedimentation of the Bakhtiyari conglomerate in the Zagros (3 Ma; Homke et al. 2004), increasing westward lateral escape rate of the Anatolian Plateau along North and East Anatolian faults (3 Ma; Allen et al. 2004) are interpreted as further evidence for this phase. In addition, the formation/reactivation of several left-lateral strike-slip faults with normal components in the west and central parts of the Alborz Mountains that cut through the Pliocene rocks since 1–1.5 Ma is considered by Ritz et al. (2006) due to a clockwise rotation of SCB. These left-lateral components of the faults are in good agreement with the earthquake focal mechanism (e.g., Vernant et al. 2004; Tatar et al. 2007; Rashidi et al. 2023), specific gravity studies (Ashtari et al. 2005), GPS data (Djamour et al. 2010), and precise levelling studies (Saberi et al. 2017) in the Central Alborz Mountains.

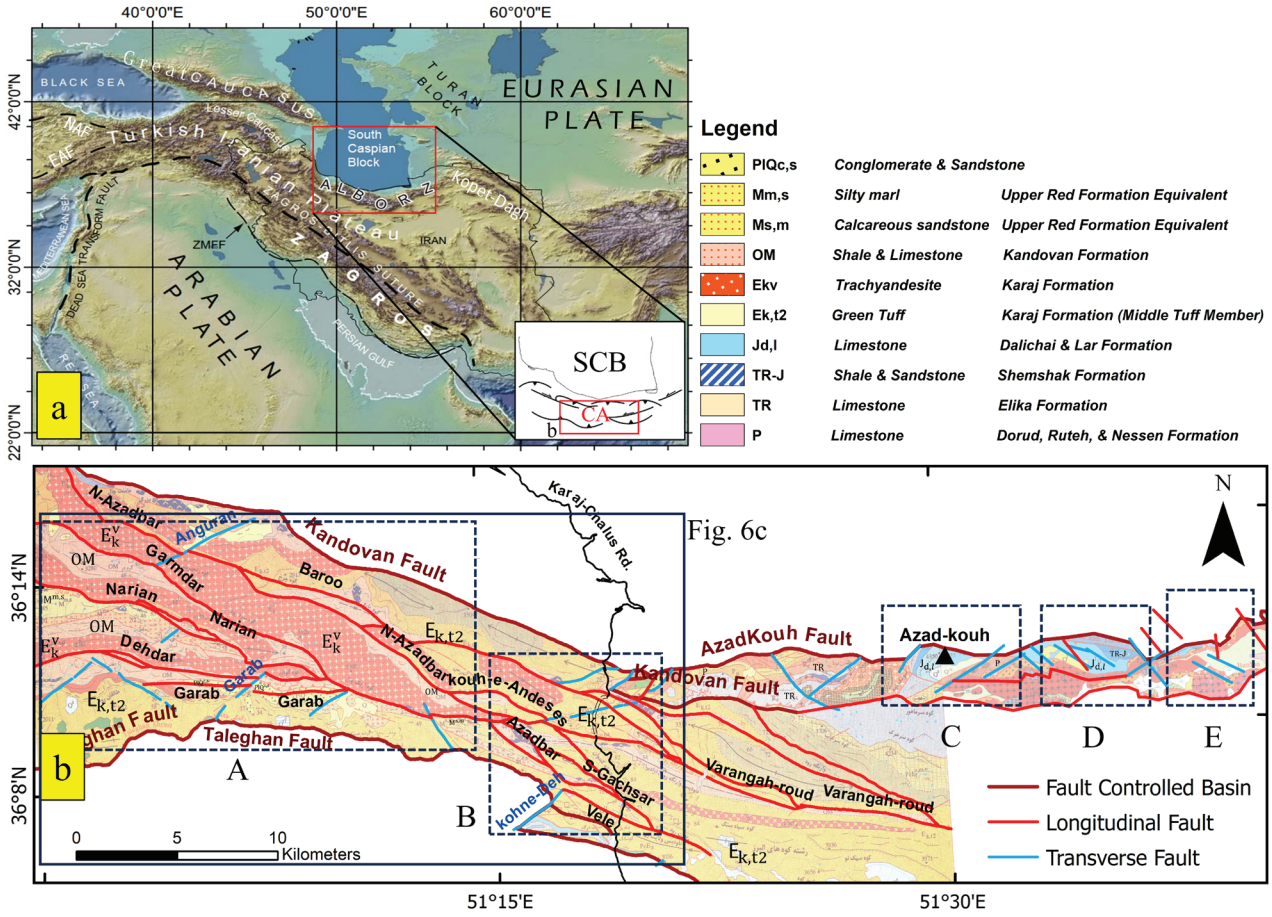

Fig. 1. a — Location of the Alborz Mountains in the convergence zone between the Arabian and Eurasian plates (revised after Guest et al. 2006 and Allen et al. 2003a). **b** — Geological map of the study area (revised after Geological Maps of the Marzan Abad; Vahdati-Daneshmand 2001) and the Baladeh (Saidi & Ghassemi 1991) in the Central Alborz Mountains showing the location of the selected areas (A–E) for faults dynamic analysis. SCB: South Caspian Block, CA: Central Alborz, NAF: North Anatolian Fault, EAF: East Anatolian Fault.

Paleostress studies in regions with complex fault geometries (like Central Alborz) could unravel their tectonic evolution (e.g., Regard et al. 2004; Zanchi et al. 2006; Navabpour et al. 2007; Zamani & Masson 2013; Javadi et al. 2015; Aflaki et al. 2021). This can be done using the Stress Inversion Method through the inversion of fault-slip data (fault kinematics; Angelier et al. 1982; Angelier 1989, 1994). Previous studies on the paleostress analysis of the Central Alborz Mountains generally considered only the main regional reverse faults (Karami 1997; Eliassi 2001; Zanchi et al. 2006; Rajabi et al. 2012). Therefore, they only recognized one compressional stress phase with an N-trending main stress axis resulting from the north-south convergence of the Arabian–Eurasian plates affected the entire Iranian Plateau. This stress state is not compatible with nowadays NNE-trending *P*-axis calculated through earthquake focal mechanisms and GPS data (e.g., Jackson et al. 2002; Ashtari et al. 2005; Ritz et al. 2006; Djamour et al. 2010). The reason for such discrepancy comes from the fact that these earlier paleostress studies did not take into account the minor strike-slip faults that cut through and displaced the main reverse faults (Yassaghi & Naeimi 2011; Fig. 1b). In this study, we reconstructed the dynamic history of the Central Alborz Mountains using both the main regional reverse faults as well as the minor strike-slip faults to show the role of the Late Cenozoic stress phases on the deformation of the Central Alborz Mountains. For this aim, a complex deformed area located between the Kandovan and Taleghan faults in the Central Alborz Mts. has been selected (Fig. 1b). Though different rock units from Paleozoic to Cenozoic are exposed in this area (Figs. 1b, 2), the faults geometry and kinematics in these rocks are identical; therefore, the rock units have suffered similar deformation phases.

Fault structures

The Kandovan and Taleghan faults form the northern and southern boundaries of the study area in the Central Alborz Mts., respectively (Figs. 1b, 2). Several minor transverse faults cutting through these faults are also mapped. The NW-striking and northeast dipping Kandovan Fault (Gansser & Hubber 1962) 200 km in length cut the tuff rocks of the Eocene Karaj

Formation and the shale and limestone of the Oligo–Miocene Kandovan Formation along most of its strike (Figs. 1b, 2a). This high-angle dip-slip fault is an inverted normal fault to reverse faulting and its inversion kinematics has been linked to the N–S shortening of the Alborz Mountains since the middle Eocene (Yassaghi 2001; Brunet et al. 2003; Zanchi et al. 2006; Yassaghi & Naeimi 2011). This is the oldest time for the Kandovan Fault compressional activity. The Kandovan fault's youngest activity turns back to Pliocene and no recent deformation evidence has been detected for the fault activity (Axen et al. 2001; Guest et al. 2006).

The NW-striking Taleghan Fault (Gansser & Hubber 1962) 100 km in length dips southwest (Fig. 1b) and puts the Jurassic and Cretaceous rock formations over the Eocene Karaj Formation in the Karaj–Chalus Road section (Fig. 2b) or over the shale and limestone of the Oligo-Miocene rocks in the Taleghan Mountain to the west of the study area (Yassaghi & Madanipour 2008). Thus, the post-Eocene reverse kinematics for the oldest fault activity is documented along its strike from the east to the west. The fault kinematics changes from the right-lateral reverse in the road's eastern part to the left-lateral reverse toward its western portion (Yassaghi & Madanipour 2008; Yassaghi & Naeimi 2011). The younger (Pleistocene–Holocene) transtensional left-lateral kinematics have also been mapped for the fault in Asara village in the Central Alborz (south of the B area in Fig. 1b; Ritz et al. 2006). Two large historical earthquakes on December 16, 1808, and November 8, 1966, with Ms=5.9 and Mb=5 in magnitude, respectively, have been attributed to the fault activity (Ambraseys & Melville 1982).

There are several other reverse faults sub-parallel to the Kandovan and Taleghan faults (Fig. 1b). These reverse faults include, for example, the Azad-kouh Fault on the hanging wall of the Kandovan Fault, as well as the North Azadbar, Dehdar, Narian, and Garmdar faults on the fault footwall (Figs. 1b, 2c–f), are imbricated from a detachment zone at the base of the Eocene Karaj Formation (Yassaghi and Naeimi 2011). A significant number of the NE- trending left-lateral transtensional faults (such as the Anguran, Dareh Garab, Lambaran, and Kohne Deh; Figs. 1b, 2g, h) truncate these reverse faults on the footwall of the Kandovan Fault. These strike-slip faults also cut and displace the Miocene–Pliocene strata. In addition, to the west of the study area, several NE-striking late Miocene (6–9 Ma) microdiorite dykes intruded into the left-lateral strike-slip faults that cut through reverse faults for about 20 m (Guest et al. 2006).

Methods

In this study, the Stress Inversion Method (Angelier et al. 1982; Angelier 1989, 1994) is employed for the paleostress analysis of the Central Alborz through the Multiple Inverse Method (MIM) Software (Yamaji et al. 2011a) using fault-slip data (i.e., fault planes and their slicken-lines attitude). This can be done by determining the reduced stress tensor that contains four independent components, including the direction of three principal stress axes ($\sigma_1 \geq \sigma_2 \geq \sigma_3$) and the ratio of their relative magnitude (Φ).

For paleostress analysis, some assumptions are generally considered as: (1) A sufficient amount of stress can lead to the formation of a new fault or reactivation of pre-existing one. In both cases, it is assumed that the sliding of the fault blocks (on the fault surface and along the slicken-side lineation) occurs parallel to the direction of the maximum shear stress (Bott 1959; Carey & Brunier 1974). (2) Fault-slip data must be gathered from various faults with different attitudes. This assumption supposes these faults formed in response to a specific stress state in a homogeneous rock body (Arthaud 1969; Carey 1976). In this study, for identifying the homogeneous rock bodies, before any processing, the homogeneity test is performed on the fault-slip data and the region was divided into homogeneous restricted areas (A–E in Fig. 1b). In practice, first, the average reduced stress tensor of the data from one of the selected locality is calculated. Then, the test proceeds by stepwise addition of nearest neighbour data to the already homogeneous data set. To call the added data set homogeneous, the changes of the newly calculated average reduced stress tensor compared to the previous steps must be negligible (i.e., the angle between average stress axes must be less than 20° and a sudden jump in the magnitude of average stress ratios (Φ) does not occur). (3) Slip on each fault is independent and does not affect the slip direction of the other faults (Carey & Brunier 1974; Angelier et al. 1982). To avoid intervention of the local stress field (caused by possible activation of the main faults, i.e., the Kandovan and Taleghan faults) on the regional stress field that affects the activity of minor and younger faults, we kept the optimal 300 m distances away from these major faults during measurements of the fault-slip data. (4) Fault planes might not have rotated after their formation, which means that the direction of the calculated principal stress axes should be parallel with the directions of ideal Andersonian stress axes at the time of fault generation/reactivation. Otherwise, before any paleostress processing, the amount of rotation must be removed. Since the amount of post-Pliocene (the youngest fault activity) rotation in the Central Alborz Mountains is not detected, for the transformation of the stress axes into the Andersonian stress state they are rotated so that the highest plunged stress axis is nearly vertical.

The MIM software includes two mim60 and miv4 programs. In the first step, the fault-slip data (column I in Fig. 3) were processed as 4-dimensional space input data in the mim60 program. Outputs of this processing are recognition of all the compatible stress tensors run in the miv4 program where the resulting stress tensors are shown as colourful points for the maximum and minimum stress axes in separate stereograms (columns II and III in Fig. 3). The colours from violet to red indicate the amount of stress ratios ($\Phi=(\sigma_2-\sigma_3)/(\sigma_1-\sigma_3)$) from 0 to 1 (with an interval of 0.1), respectively. Each colour cluster (indicated by a small black circle in the stereograms of Fig. 3) also shows a stress phase. Accepting or

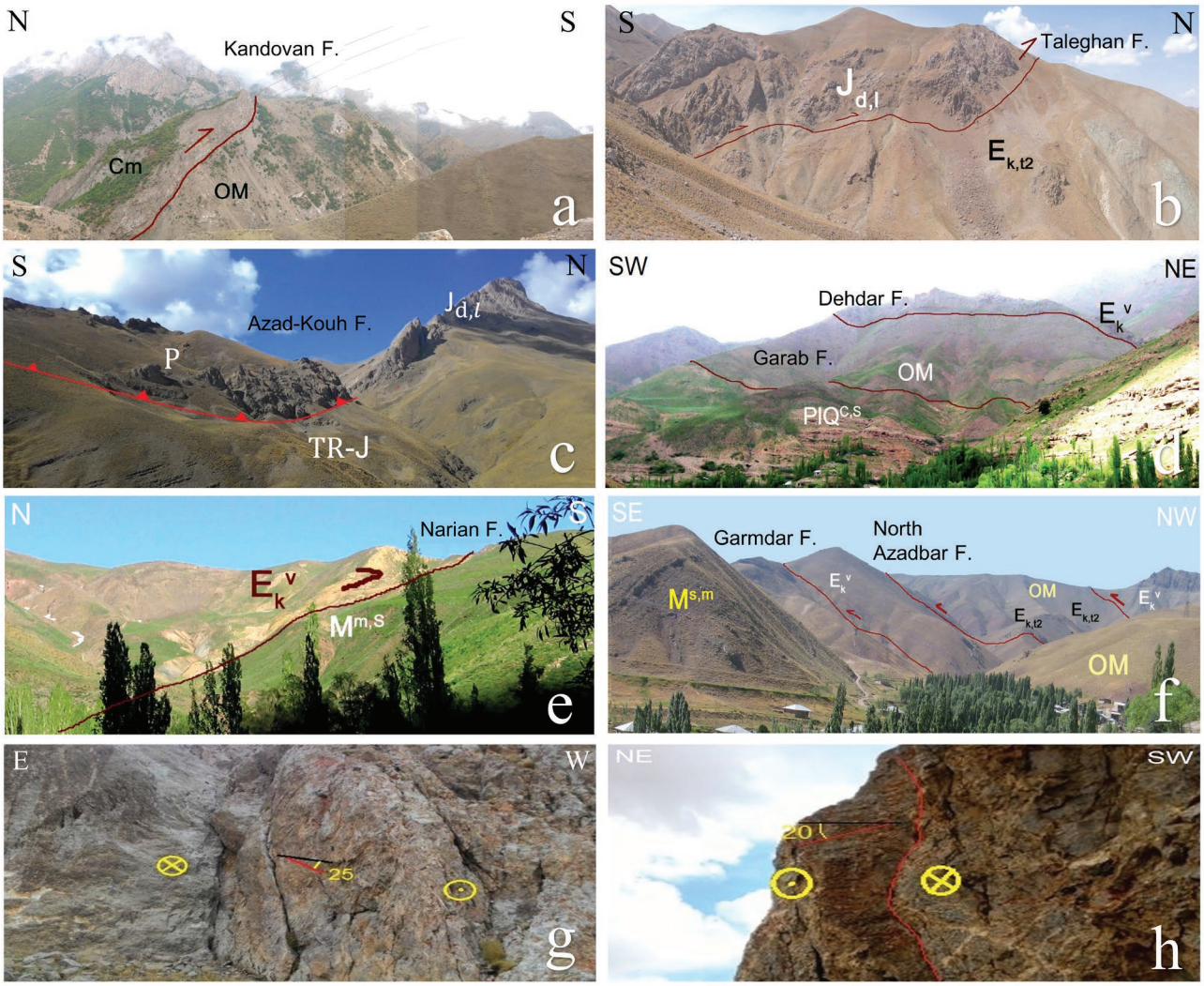

Fig. 2. Field photographs of (**a–f**) the reverse faults and (**g–h**) the NE-trending left-lateral strike-slip faults in the Central Alborz Mountains. Cm: Carboniferous (Mobarak Formation, out of the study area), P: Permian, TR-J: Triassic–Jurassic (Shemshak Formation), $J_{d,l}$: Jurassic (Dalichai and Lar formations), $E_{k,t2}$, E_k^v: Eocene (Tuff and Volcanic rocks of the Karaj Formation), OM: Oligo-Miocene (Kandovan Formation), $M^{s,m}$, $M^{m,s}$: Miocene (Upper Red Formation equivalent), $PlQ^{c,s}$: Pleistocene. The photographs (a–b and d–f) from Naeimi (2007) and (c, g–h) from Barati (2017). Refer to Fig. 1b for the locations of the faults and the rock formations.

rejecting the clusters as possible stress phases is based on the interpretation of a user upon the study area. Through these phase selections, faults-slip data that documents different stress phases will be separated manually using Yamaji et al. (2011b) criterion into certain phases and their related reduced stress tensor will be calculated.

With specific stress axes orientations (a stress state) that act on a certain fault plane (Fig. 4), two end members for the orientation of the slicken-lines (parallel to the maximum shear stress, see first paleostress assumption) from $\tau_0(\Phi=0)$ to $\tau_1(\Phi=1)$ is predictable. This can be used for the determination of the range of the possible fault mechanisms for a certain

Fig. 3. Characteristics of the 10 selected stress phases in this study. I – Stereograms show the attitude of the fault-slip data (arrows show their movement directions). II and III – Demonstration of the principal orientations of the paleostress axes plotted in stereographic projections (lower-hemisphere, equal-area projection) measured in the selected areas. They are the stress states which are compatible, at least, with one single data in each area. Lengths of the tails of tadpole symbols denote the plunge of paleostress axes. Φ values are colour-coded with intervals of 0.1. Black circles and numbers show selected phases. IV – The non-scaled Mohr diagrams were drawn to compare the slip tendency ($T_S=|\tau|/|\sigma_n|$) among compatible fault-slip sets in each phase. The drawn coloured circles and ellipsoids for the selected data present different fault mechanisms shown as legends at the bottom of the figure. The histograms below the Mohor diagrams present the amount of misfit angles for the selected paleostress phases. For the locations of the studied areas in the Central Alborz Mountains, refer to Fig. 1b.

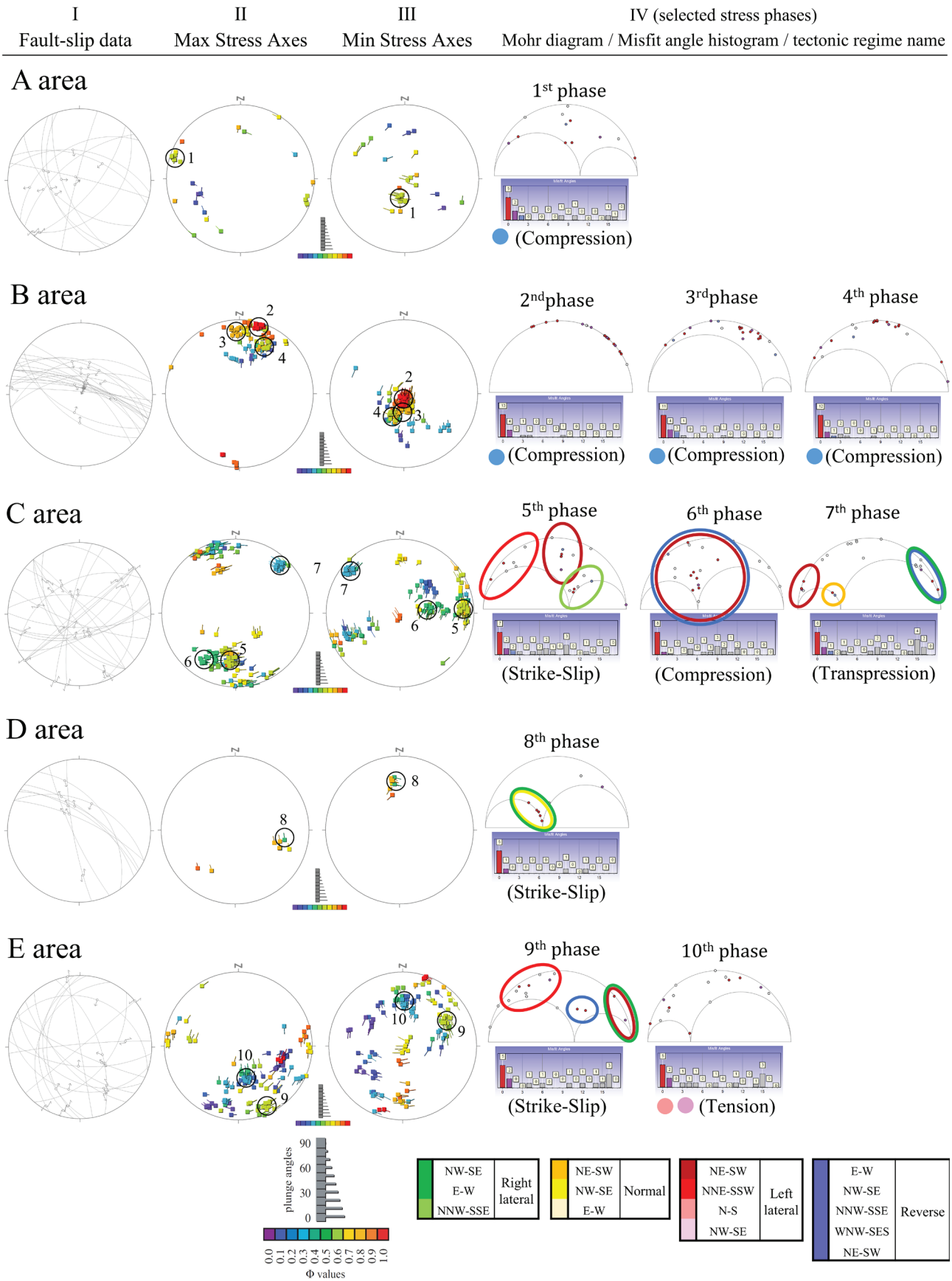
I
Fault-slip data
II
Max Stress Axes
III
Min Stress Axes
IV (selected stress phases)
Mohr diagram / Misfit angle histogram / tectonic regime name
A area
1st phase
(Compression)
B area
2ndphase
3rdphase
4th phase
(Compression)
(Compression)
(Compression)
C area
5th phase
6th phase
7th phase
(Strike-Slip)
(Compression)
(Transpression)
D area
8th phase
(Strike-Slip)
E area
9th phase
10th phase
(Strike-Slip)
(Tension)
plunge angles
90
60
30
0
Φ values
0.0 0.1 0.2 0.3 0.4 0.5 0.6 0.7 0.8 0.9 1.0
NW-SE
E-W
NNW-SSE
Right lateral
NE-SW
NW-SE
E-W
Normal
NE-SW
NNE-SSW
N-S
NW-SE
Left lateral
E-W
NW-SE
NNW-SSE
WNW-SES
NE-SW
Reverse

Fig. 4. Stereogram shows possible orientations for slicken-lines that fall between τ_0 and τ_1 for a fault plane (F) affected by a specific stress state. In this example, the fault kinematics can change from pure reverse to right-lateral reverse.

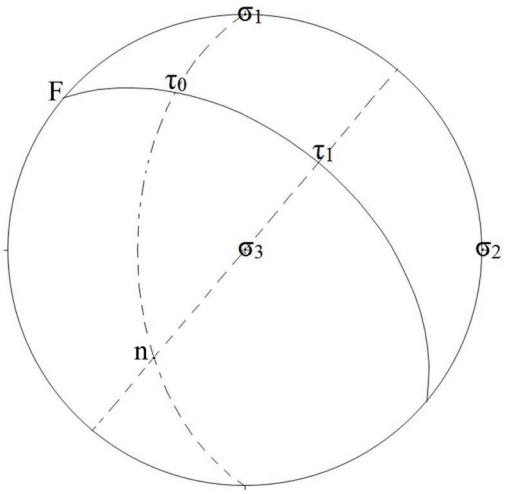

fault plane (Fig. 4). In fact, this possible range of the slicken-side lineation from τ_0 to τ_1 highlights the effect of the magnitude of stress ratio ($0 \leq \Phi \leq 1$) on fault mechanism when the orientations of stress axes are fixed. In this study to realize the admissibility of the recognized stress phases, the compatibility of the interpreted fault mechanisms (fault-slip data) with the selected phases (including the magnitude of stress ratio (Φ) and specific orientations for principal stress axes) was checked (Table 1).

Result

The study region is divided into five restricted areas from A to E from the west to the east (Fig. 1b) based on the homogeneity test on the fault-slip data. For each restricted area, stress phases, which were demonstrated as a colourful cluster in MIM software, were manually selected (the 10 selected phases by the small black circles drawn in the stereograms;

Table 1: Presentation of the attitude of principle stress axes orientations, the stress ratio magnitude (Φ) for each selected phase as well as their compatible faults' kinematics and their tectonic regime in each selected area.

Area	Phase	Sigma 1		Sigma 2		Sigma 3		Phi	Tectonic Regime	Mechanism	Strike
		Trend	Plunge	Trend	Plunge	Trend	Plunge				
A	1	287.9	3.5	19.1	20.8	188.5	69.1	0.6	Compression	Reverse	NNW–SSE WNW–SES NE–SW
B	2	15	6.3	284.8	1	184.9	83.7	1	Radial Compression	Reverse	NW–SE
	3	356.2	18.3	265	3	166.5	71.4	0.8			
	4	29.5	25.9	120	1	211.8	64.1	0.6	Compression		
C	5	186.9	34.1	332.7	50.8	84.8	17.2	0.6	Strike-Slip	Left lateral	NNE–SSW NE–SW
										Reverse Normal	E–W
										Right lateral	NNW–SSE
	6	214.8	23.1	314.4	21.4	82.6	57.6	0.4	Compression	Reverse	NW–SE E–W NE–SW
										Left lateral	NE–SW
	7	42.8	14.4	182	71.5	309.8	11.7	0.3	Transpression	Left lateral Normal	NE–SW
										Reverse Right lateral	NW–SE
D	8	106	32.8	228.5	40	351.5	32.9	0.4	Strike-Slip	Normal Left lateral Right lateral	NW–SE
E	9	154.4	10.5	260	55.7	57.5	32.4	0.6	Strike-Slip	Left lateral	NNE–SSW NE–SW
										Reverse	NW–SE NE–SW
										Right lateral	E–W
	10	165.6	50.9	266	8	2.1	38	0.3	Radial Tension	Left lateral	N–S NNE–SSW NW–SE
										Normal	NW–SE

Fig. 3). In addition, for each stress phase (Fig. 3), the direction of stress axes, the amount of stress ratio (Φ), and its potentially compatible faults have determined (Table 1).

Outcomes of a specific stress phase (Fig. 3; Table 1) out of the MIM software might be compatible with several fault sets. Although it is acceptable in theory, in practice, slips on a fault set, prevent the stress accommodation on the other fault sets. Generally, fault planes are more likely to form or reactivate if the angle between their normal and maximum stress axes is $15°<\theta<75°$(Donath 1972). In other words, the resulting shear stress on these fault planes must be greater than the other fault sets (Slip Tendency). This tendency to slip ($T_S=|\tau|/|\sigma_n|$; Morris et al. 1996) for the compatible fault sets within each stress phase can be explained by using non-scaled Mohr diagrams. Each fault set with a higher shear stress relative to normal stress denotes its higher slip tendency, which means that the fault set is more likely to shear by the interpreted stress phase. Such Mohr diagrams for all the 10 selected phases are presented in Fig. 3 (column IV). For the phases that are compatible with more than one fault set, their slip tendencies were compared and the best set(s) were selected. The result of this process for the fault-slip data in the study areas is presented in the following.

The NW-striking reverse faults are the compatible faults for the selected phases Nos. 1 to 4 in the A and B areas (Figs. 1b, 3; Table 1). For the selected phases Nos. 5 to 7 considered for the C area (Figs. 1b, 3; Table 1), the NNE-striking sinistral strike-slip faults and the NE-striking left-lateral transtensional faults show higher slip tendency in the non-scaled Mohr diagrams of 5th and 7th phases, respectively (Fig. 3). The 6th phase is compatible with the W- and NW-striking reverse faults as well as the NE-striking left-lateral strike-slip faults (Fig. 3; Table. 1). For the D area (Fig. 1b; Table 1) phase No. 10 has been selected with compatible NNW-striking left-lateral transtensional faults (Fig. 3; Table 1). Finally, for the E area (Figs. 1b), phases Nos. 9 and 10 are selected (Fig. 3; Table 1). For the 9th phase based on fault-slip tendency criteria (Non-scaled Mohr Diagram in Fig. 3), the NE-striking left-lateral strike-slip faults were selected whereas for the 10th phase the N- to NW-striking left-lateral transtensional faults are considered as compatible faults.

The results of paleostress reconstruction can be summarized in three main groups of stress phases. For the A, B and C areas (Fig. 1b), the stress phases Nos. 1–4, and 6 (Fig. 3; Table 1) are compatible with the vertical σ_3, N- to NE-trending horizontal σ_1, and medium to high-stress ratio (Φ=0.4–1) are inferred to be responsible for the formation of the NW–SE oriented reverse faults (Figs. 2a–f, 3; Table 1). The 6th and 7th stress phases (Fig. 3; Table 1) in the C area (Figs. 1b) which are compatible with the NE-trending horizontal σ_1 and medium magnitude of the stress ratio (Φ=0.3–0.4) are responsible for the formation of the NE-striking left-lateral strike-slip faults (Figs. 2g–h, 3). The stress phases Nos. 5, 8, 9, and 10 (Fig. 3) in the C, D, and E areas (Fig. 1c) are compatible with approximately S-trending horizontal σ_1 and low to medium magnitude of the stress ratio (Φ = 0.3–0.6; Fig. 3). These phases are responsible for formation of almost N-striking (NNE to NNW) left-lateral transtensional faults (Fig. 3; Table 1).

Discussion

According to the Andersonian state of stress (Anderson 1951), once one of the maximum, medium, or minimum principal stress axes is vertical or sub-vertical, the tectonic regime will be extensional, strike-slip, or compressional, respectively. Based on the attitude of principal stress axes and the value of stress ratio (Φ) extracted from the MIM software (the colourful clusters in Fig. 3), the selected stress phases can be referred to proper tectonic regimes (Table 1; Fig. 3). The drawn rose-diagrams for the attitude of the reverse, normal, and strike-slip faults in the study area (Fig. 5) show that the NW–SE reverse faults (dipping about 40°) have the highest frequency. The NE-striking left-lateral strike-slip faults all dipping greater than 70° as well as the NW–SE normal faults (dipping 60°) and right-lateral strike-slip faults have the next order of frequency (Fig. 5). Results on the admissibility of the recognized stress phases (Fig. 3; Table 1) provide data to propose that the reverse, left-lateral strike-slip, and left-lateral transtensional faults might have activated by its stress phase. Therefore, upon the results of these analyses, three distinct compressional, transpressional, and transtensional tectonic phases are proposed.

Compressional tectonic regime

The interpreted N- to NE-trending horizontal σ_1 (stress phases Nos. 1–4 and 6 in Fig. 3; Table 1) for the range parallel reverse faults in the Central Alborz Mountains (Figs. 1, 2a–f, 5a) are compatible with a compressional deformation regime. Based on Anderson's (1951) criterion, considering the internal friction angle of rock masses as 30–40°, the dip angle of the reverse, normal and strike-slip faults within the competent rock will be 30, 60 and 90 degrees, respectively. Upon Fig. 5, the highest deviation on dip angle from this criterion refers to the reverse faults. Since the Eocene Karaj Formation with almost uniform mechanical properties is the main rock mass in the Central Alborz Mountains (Figs. 1b, 2), this deviation is proposed to be rooted in the older deformation history of the reverse faults.

It is generally believed that the reverse faults in the Alborz Mountains are formed by a compressional tectonic regime (Allen et al. 2003a; Guest 2004; Guest et al. 2007; Yassaghi & Naeimi 2011). Paleomagnetic data indicate the formation of the mountains, under the compressional tectonic regime with the N- trending principal maximum paleostress axis (σ_1) during the Miocene which replaced older Eocene extensional tectonic regime (Cifelli et al. 2015) provide further evidence for this interpretation. Thus, inversion of the initial normal faults such as the regional (Kandovan and Taleghan) faults to reverse ones (e.g., Yassaghi & Madanipour 2008; Yassaghi &

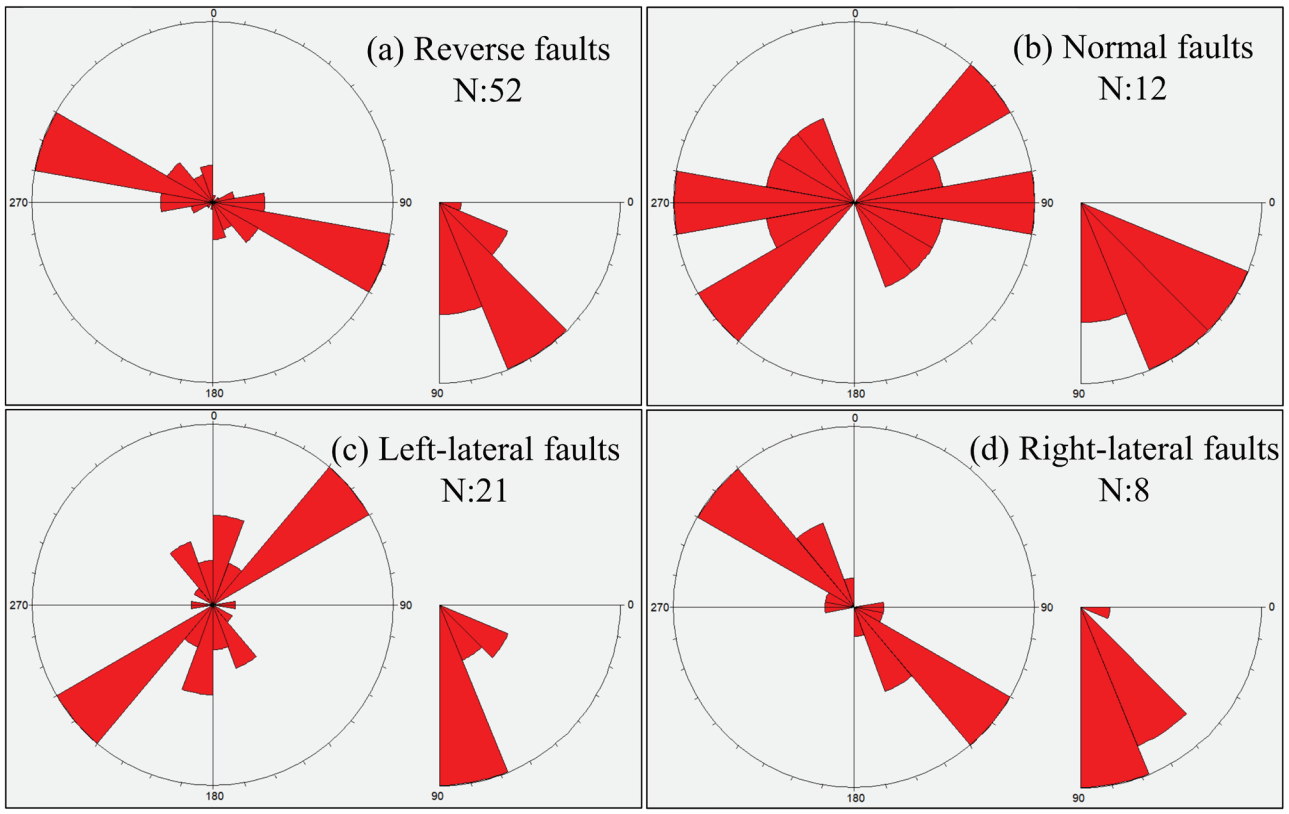

Fig. 5. Rose diagrams on orientation (left diagrams) and dip angle (right diagrams) of faults-slip data for (**a**) reverse, (**b**) normal, (**c**) left-lateral strike-slip and (**d**) right-lateral strike-slip faults. N: amount of data.

Naeimi 2011) might have occurred during this compressional tectonic phase. Since these reverse faults are cross-cut by the NE–SW strike-slip faults (Fig. 6c), this compressional regime is interpreted as older than the later strike-slip tectonic regime in the Central Alborz Mountains.

Transpressional tectonic regime

The NE-trending horizontal σ_1 (stress phases Nos. 6–7 in Figs. 3, Table 1) responsible for the formation of the NE-striking left-lateral strike-slip faults like the Karaj–Chalus Valley Fault (Fig. 6c, d) are compatible with the transpressional tectonic regime. These faults have been interpreted to be the result of reactivation of the Alborz Mountains' basement faults like the F-3 magnetic fault (Fig. 6b, c) as R-Riedel shear faults on the cover rocks (Yassaghi & Naeimi 2011). Similarly, the NE-striking Karaj–Chalus Valley, Anguran, Lambaran, and Garab Valley faults are also proposed as the Riedel shear faults related to the reactivation of the F-3 magnetic Fault (Fig. 6c, d). Thus, the reactivation of this basement fault is interpreted as a result of changes in the direction of the maximum paleostress axis from the North-trending (in the compressional regime) to the NE-trending (in the transpressional regime).

The required differential stress (σ_1–σ_3) for reactivation of a strike-slip fault is much less than that of a reverse fault (Fossen 2016) especially for a high-angle dip one like the regional reverse faults in the study area (Figs. 5a, 6c). The angle between NE-trending σ_1 of the transpressional regime (6th and 7th phases in Fig. 3) and the NE–SW basement faults (F-3 in Fig. 6b) falls in the reactivation range of $15° < \theta < 75°$(Donath 1972) whereas for the range parallel reverse faults fall out of this ideal state. Thus, it can be proposed that rotation of the maximum paleostress axis (σ_1) from the N-trending compressional to the NE-trending transpressional regime in the Central Alborz Mountains more likely reactivated the basement faults (resulted in the development of the Karaj–Chalus Valley and the Qazvin dentation faults in the sedimentary cover) than the regional reverse faults (Fig. 6). This reactivation is more effective in the B and C areas (Fig. 1b) which are closer to the Karaj–Chalus Valley Fault and thus its activity induced the structures to rotate passively around an E-horizontal axis which resulted in a higher angle dip of the reverse faults in these areas (Figs. 5a, 6e). Evidence on such passive rotation due to the reactivation of the F-3 magnetic fault has also reported from the changes of the fold axes attitude in the B area (Yassaghi & Naeimi 2011).

Displacement of the reverse faults and the middle Miocene and Pliocene rock units by the NE–SW-oriented left-lateral strike-slips faults (Figs. 1b, 6c) provide support to conclude that this transpressional tectonic regime is younger than the compressional one. The change in the tectonic regime from

compressional to transpressional might have occurred by a regional actor. It is generally believed that SCB indentation into the Iranian Plateau has occurred during the convergence of the Arabian and Eurasian plates at about 6 Ma (Axen et al. 2001), 5 Ma (Jackson et al. 2002; Allen et al. 2003a, b), or 3 Ma (Allen et al. 2004). Approximately 15–20° rotation of magnetic mineral around a vertical axis in rock layers subparallel to the Alborz Mountains trend and inception of the mountains bending has also been related to the indentation of SCB (Ballato et al. 2008; Cifelli et al. 2015; Mattei et al. 2017). In addition, the Pliocene Alam-kouh granite (~6.8 Ma; Axen et al. 2001) that cut the Kandovan Fault west of the Central Alborz Mountains (Guest 2004) is the other evidence for the syn-tectonic penetration of this indentation. This episode proposed for the uplift and deformation in the Zagros, Alborz and Talesh in the Iranian Plateau as well as in the north and west of the Anatolian Plateau as the result of the acceleration in spreading of the Red Sea floor and its oceanic lithosphere inception (Axen et al. 2001; Allen et al. 2003a, b). Thus, the analyzed transpressional tectonic regime for the Central Alborz Mountains has been effective since the Pliocene across the Arabian–Eurasian continental collision zone.

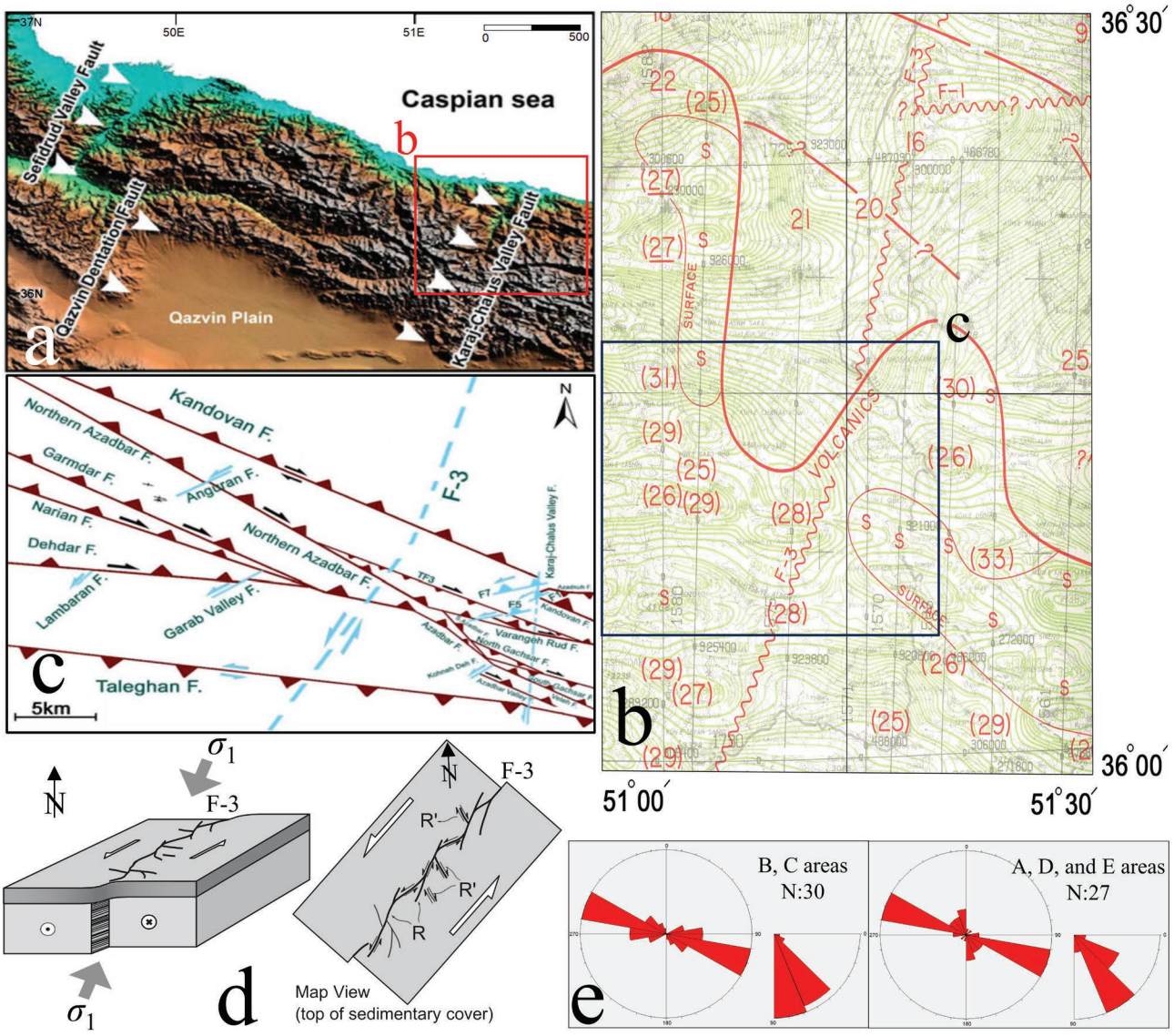

Fig. 6. a — 3D image of the central Alborz Mountains showing the location of the major left-lateral strike-slip faults. **b** — The aeromagnetic map shows the location of the F-1 and F-3 magnetic faults (Yousefi & Friedberg 1977). **c** — Structural map of the study area (Yassaghi & Naeimi 2011). **d** — 3D diagram and its map view showing reactivation of the F-3 magnetic basement fault as the Riedel shear fractures on the sedimentary cover (like the Karaj–Chalus Valley Fault on Fig. 6a). **e** — Rose diagrams for the strikes (left diagrams) and dip angles (right diagrams) of the reverse faults in the B and C areas located close to the Karaj–Chalus Valley Fault and in the A, D, and E areas located further (refer to Fig. 1b for the location of the areas). N: amount of data.

Transtensional tectonic regime

The horizontal and N–S maximum paleostress axis (σ_1) (stress phases Nos. 5, 9, and 10 in Fig. 3; Table 1) is proposed to be responsible for the initiation of the NNE- to NNW-striking left-lateral strike-slip with normal component faults originated under a transtensional deformation regime. These faults cut and displaced the Quaternary Damavand volcanic rocks (Saberi et al. 2017) are more likely *P*-Riedel shear faults resulting from the reactivation of the NE–SW basement faults (like the F-3 magnetic fault in Fig. 6b).

Morphotectonics and paleo-seismological evidence along the Fioruz-kouh, Astaneh, Bashm, Chashm, Sorkh-e Hesar, Ghasr-e-Firuzeh, eastern part of the Mosha, North Tehran, and Taleghan faults (Ritz et al. 2006; Nazari et al. 2009; Mohammadi Nia et al. 2023) show their recent kinematics as left-lateral with normal component. Satellite images also show about 3 km left-lateral horizontal displacements for the river catchments crossing the faults. By extrapolation of the present-day GPS rate to the past, we propose this deformational regime has been acting since the Pleistocene coeval with the latest activity of the Damavand Volcano (1.8 Ma – 7 ka; Davidson et al. 2004). This interpretation is also in agreement with the proposed left-lateral strike-slip focal mechanism for recent earthquake faults epi-centered along the NNW- and WSW-striking faults in Central Alborz Mountains (Ashtari et al. 2005). Similarly, the NE–SW left-lateral strike-slip focal mechanism for the 28 May 2004 Balade aftershock with Mw=6.2 magnitude in the Central Alborz (Tatar et al. 2007) is also proposed here as to the recent activity for this transtensional tectonic regime. These morphotectonics and paleo-seismological evidence are referred to because of the clockwise rotation of SCB relative to the Alborz Mountains since 1–1.5 Ma (Ritz et al. 2006). Accordingly, we concluded that the proposed transtensional regime is the youngest one governed by the Central Alborz Mountains.

Conclusion

Paleostress reconstruction of the fault-slip data in the Central Alborz Mountains resulted in the recognition of three main tectonic regimes. The paleostress phases Nos. 2–4 with an almost N-oriented horizontal maximum paleostress axis (σ_1) is proposed to be responsible for the formation of the WNW–ESE reverse faults. These phases are compatible with a compressional regime acted in the mountains during the convergence of the Arabian–Eurasian plates.

The paleostress phases Nos. 5–7 with the NE–SW-oriented horizontal maximum paleostress axis (σ_1) is suggested due to a transpressional tectonic regime in which the NE–SW left-lateral basement faults have triggered to reactivate and resulted in the evolution of the left-lateral R-Riedel shear faults on the sedimentary cover. These faults cut and displaced the preexisted reverse faults. This tectonic regime has caused the indentation of SCB into the Iranian Plateau during the convergence of the Arabian and Eurasian plates.

The paleostress phase Nos 8–10 with SE-oriented horizontal maximum paleostress axis (σ_1) caused the formation of the general NNE- to NNW-trending left-lateral strike-slip faults with the normal component. This faulting that is compatible with earthquake focal mechanisms, as well as active vertical movements in the Central Alborz Mountains, is formed in a transtensional tectonic regime more likely during the clockwise rotation of SCB in Quaternary.

Analysis of the fault-slip tendency using the non-scaled Mohr diagrams shows that the NW-trending reverse faults do not tend to slip whereas the NE-trending left-lateral strike-slip faults formed/reactivated during transpressional or transtensional tectonic regime show slip tendency which reflect their ability to act as active faults.

Acknowledgements: The authors acknowledge the financial support of Tarbiat Modares University during the fieldwork. The authors also acknowledge Rastislav Vojtko, the associated editor as well as Viera Šimonová and the other anonymous reviewer for their generous and insightful review comments, which greatly improved the manuscript. We thank Silvia Antolíková, Managing Editor for editorial handling.

Reference

Aflaki M., Shabanian E., Sahami S. & Arshadi M. 2021: Evolution of the stress field at the junction of Talesh–Alborz–Central Iran during the past 5 Ma: Implications for the tectonics of NW Iran. *Tectonophysics* 821, 229115. https://doi.org/10.1016/j.tecto.2021.229115

Alavi M. 1996: Tectonostratigraphic synthesis and structural style of the Alborz Mountain System in Iran. *Journal of Geodynamics* 21, 1–33. https://doi.org/10.1016/0264-3707(95)00009-7

Allen M.B., Ghassemi M.R., Shahrabi M. & Qorashi M. 2003a: Accommodation of late Cenozoic oblique shortening in the Alborz range, northern Iran. *Journal of Structural Geology* 25, 659–672.

Allen M.B., Vincent S.J., Alsop G.I., Ismail-zadeh A. & Flecker R. 2003b: Late Cenozoic deformation in the South Caspian region: effects of a rigid basement block within a collision zone. *Tectonophysics* 366, 223–239. https://doi.org/10.1016/S0040-1951(03)00098-2

Allen M., Jackson J. & Walker R. 2004: Late Cenozoic reorganization of the Arabia-Eurasia collision and the comparison of short-term and long-term deformation rates. *Tectonics* 23, TC2008. https://doi.org/10.1029/2003TC001530

Ambraseys N.N. & Melville C.P. 1982: A history of Persian earthquakes. Cambridge Earth Science Series. *Cambridge University Press*, London.

Anderson E.M. 1951: The Dynamics of Faulting and Dyke Formation with Applications to Britain. 2nd ed., *Oliver and Boyd*, Edinburgh.

Angelier J. 1989: From orientation to magnitude in paleostress determination using fault slip data. *Journal of Structural Geology* 11, 37–50. https://doi.org/10.1016/0191-8141(89)90034-5

Angelier J. 1994: Fault slip analysis and palaeostress reconstruction. In: Hancock P.L. (Ed.): Continental deformation. *Pergamon press*, Oxford, 53–100.

Angelier J., Tarantola A., Valette B. & Manoussis S. 1982: Inversion of field data in fault tectonics to obtain the regional stress – I. Single phase fault populations: a new method of computing the stress tensor. *Geophysical Journal* 69, 607–621. https://doi.org/10.1111/j.1365-246X.1982.tb02766.x

Annells R.N., Arthurton R.S., Bazley R.A. & Davies R.G. 1975: Explanatory text of Qazvin and Rasht quadrangles map. *Geological Survey of Iran*, Tehran.

Arthaud F. 1969: Determination graphique des directions de raccourcissement, d'allongeent et intermediaire d'une population de failles. *Society of Geology of France* 7, 729–737.

Ashtari M., Hatzfeld D. & Kamalian N. 2005: Microseismicity in the region of Tehran. *Tectonophysics* 395, 193–208. https://doi.org/10.1016/j.tecto.2004.09.011

Axen G.J., Lam P.S., Grove M., Stockli D.F. & Hassanzadeh J. 2001: Exhumation of the west-central Alborz Mountains, Iran, Caspian subsidence, and collision-related tectonics. *Geology* 29, 559–562. https://doi.org/10.1130/0091-7613(2001)029<0559:EOTWCA>2.0.CO;2

Ballato P., Nowaczyk N.R., Landgraf A., Strecker M.R., Friedrich A. & Tabatabaei S.H. 2008: Tectonic control on sedimentary facies pattern and sediment accumulation rates in the Miocene foreland basin of the southern Alborz Mountains, northern Iran. *Tectonics* 27, TC6001. https://doi.org/10.1029/2008TC002278

Ballato P., Stockli D.F., Ghassemi M.R., Landgraf A., Strecker M.R., Hassanzadeh J., Friedrich A. & Tabatabaei S.H. 2013: Accommodation of transpressional strain in the Arabia-Eurasia collision zone: new constraints from (U–Th)/He thermochronology in the Alborz Mountains, north Iran. *Tectonics* 32, 1–18. https://doi.org/10.1029/2012TC003159

Barati M.A. 2017: Geometry and kinematic analysis of Azad-kouh fault zone in central Alborz. *M.Sc. thesis, Tarbiat Modares University*.

Berberian M. 1983: The southern Caspian: A compressional depression floored by a trapped, modified oceanic crust. *Canadian Journal of Earth Science* 20, 163–183. https://doi.org/10.1139/e83-015

Bott M.H.P. 1959: The mechanism of oblique slip faulting. *Geology* 96, 109–117. https://doi.org/10.1017/S0016756800059987

Brunet M.-F., Korotaev M.V., Ershov A.V. & Nikishin A.M. 2003: The South Caspian Basin: a review of its evolution from subsidence modelling. *Sedimentary Geology* 156, 119–148. https://doi.org/10.1016/S0037-0738(02)00285-3

Carey E. & Brunier B. 1974: Analysis theorique et numerique d'un modele mecanique elementaire applique a l'etude d'une population de failles. *Paris Academie de Scinces Comptes Rendus, Ser. D* 288, 891–894.

Carey E. 1976: Analyse numerique d'un modele mecanique elementaire applique a l'Etude d'une Population de Failles: Calcul d'un tenseur moyen des contraintes a partir de Stries de Glissement. *These 3e cycles, Tectonique generale*, Paris-Sud.

Cifelli F., Ballato P., Alimohammadian H., Sabouri J. & Mattei M. 2015: Tectonic magnetic lineation and oroclinal bending of the Alborz range: Implications on the Iran-Southern Caspian geodynamics. *Tectonics* 34, 116–132. https://doi.org/10.1002/2014TC003626

Davidson J., Hassanzadeh J., Berzins R., Stockli D.F., Bashukooh B., Turrin B. & Pandamouz A. 2004. The geology of Damavand volcano, Alborz Mountains, northern Iran. *Geological Society of America Bulletin* 116, 16–29. https://doi.org/10.1130/B25344.1

Djamour Y., Vernant P., Bayer R., Nankali H.R., Ritz J.-F., Hinderer J., Hatam Y., Luck B., Le Moigne N., Sedighi M. & Khorrami F. 2010: GPS and gravity constraints on continental deformation in the Alborz Mountain range, Iran. *Geophysical Journal International* 183, 1287–1301. https://doi.org/10.1111/j.1365-246X.2010.04811.x

Donath F.A. 1972: Effects of cohesion and granularity on deformational behaviour of anisotropic rock. *Geological Society of America*, *Memoirs* 135, 95–128.

Eliassi M. 2001: Fault slip analysis for determination of paleostress tensor and type of deformation in southern part of the Central Alborz. *Ph.D. Thesis, Tarbiat Modares University* (in Persian).

Fossen H. 2016: Structural Geology. *Cambridge University Press*, London.

Gansser A. & Hubber H. 1962: Geological observations in the Central Elburz, Iran. *Schweizerische Mineralogische und Petrographische Mitteilungen* 42, 583–630.

Guest B. 2004: The thermal, sedimentological and structural evolution of the central Alborz Mountain of northern Iran: Implications for the Arabia-Eurasia continent-continent collision and collisional processes in general. *Ph.D. thesis, University of California*.

Guest B., Axen G.J., Lam P.S. & Hassanzadeh J. 2006: Late Cenozoic shortening in the west-central Alborz Mountains, northern Iran, by combined conjugate strike-slip and thin-skinned deformation. *Geosphere* 2, 35–52. https://doi.org/10.1130/GES00019.1

Guest B., Horton B.K., Axen G.J., Hassanzadeh J. & McIntosh W.C. 2007: Middle to Late Cenozoic basin evolution in the western Alborz Mountains: Implications for the onset of collisional deformation in northern Iran. *Tectonics* 26, 1–26. https://doi.org/10.1029/2006TC002091

Homke S., Vergés J., Garcés M., Emami H. & Karpuz R. 2004: Magnetostratigraphy of Miocene–Pliocene Zagros foreland deposits in the front of the Push-e Kush Arc (Lurestan Province, Iran). *Earth and Planetary Science Letters* 225, 397–410. https://doi.org/10.1016/j.epsl.2004.07.002

Jackson J., Priestley K., Allen M. & Berberian M. 2002: Active tectonics of the South Caspian Basin. *Geophysical Journal International* 148, 214–245. https://doi.org/10.1046/j.1365-246X.2002.01588.x

Javadi H.R., Esterabi Ashtiani M., Guest B., Yassaghi A., Ghassemi M.R., Shahpasandzadeh M. & Naeimi A. 2015: Tectonic reversal of the western Doruneh Fault System: Implications for Central Asian tectonics. *Tectonics* 34, 2034–2051. https://doi.org/10.1002/2015TC003931

Karami H.R. 1997: Determination of paleostress and thrusting in the north of Tehran (Between Darakeh valley and Kan valley). *M.Sc. thesis, Tarbiat Modares University* (in Persian).

Mattei M., Cifelli F., Alimohammadian H., Rashid H., Winkler A. & Sagnotti L. 2017: Oroclinal bending in the Alborz Mountains (Northern Iran): New constraints on the age of South Caspian subduction and extrusion tectonics. *Gondwana Research* 42, 13–28. https://doi.org/10.1016/j.gr.2016.10.003

Mohammadi Nia A., Rashidi A., Khatib M.M., Mousavi S.M., Nemati M., Shafieibafti S. & Derakhshani R. 2023: Seismic Risk in Alborz: Insights from Geological Moment Rate Estimation and Fault Activity Analysis. *Applied Sciences*, 13, 6236. https://doi.org/10.3390/app13106236

Morris A., Ferrill D.A. & Henderson D.B. 1996: Slip-tendency analysis and fault reactivation. *Geology* 24, 275–278. https://doi.org/10.1130/0091-7613(1996)024<0275:STAAFR>2.3.CO;2

Naeimi A. 2007: Geometry and kinematic analysis of the thrust fault system between Kandovan and Taleghan faults in Azadbar area (central Alborz). *M.Sc. Thesis, Tarbiat Modares University* (in Persian).

Navabpour P., Angelier J. & Barrier E. 2007: Cenozoic post-collisional brittle tectonic history and stress reorientation in the High Zagros Belt (Iran, Fars Province). *Tectonophysics* 432, 101–131. https://doi.org/10.1016/j.tecto.2006.12.007

Nazari H., Ritz J.-F., Salamati R., Shafei A., Ghassemi A., Michelot J.-L., Massault M. & Ghorashi M. 2009: Morphological and palaeoseismological analysis along the Taleghan fault (Central

Alborz, Iran). *Geophysical Journal International* 178, 1028–1041. https://doi.org/10.1111/j.1365-246X.2009.04173.x

Rajabi S., Eliassi M. & Saidi A. 2012: Statistic and genetic investigation of faults in North Tehran. *Arabian Journal of Geoscience* 5, 1269–1277. https://doi.org/10.1007/s12517-010-0270-7

Rashidi A., Nemati M., Shafieibafti S., Pourbeyranvand A., Derakhshani R. & Braitenberg C. 2023: Structure and kinematics of active faulting in the northern domain of Western and Central Alborz, Iran and interpretation in terms of tectonic evolution of the region. *Journal of Asian Earth Sciences* 255, 105760. https://doi.org/10.1016/j.jseaes.2023.105760

Regard V., Bellier O., Thomas J.-C., Abbassi M.R., Mercier J., Shabanian E., Feghhi K. & Soleymani S. 2004: Accommodation of Arabia-Eurasia convergence in the Zagros-Makran transfer zone, SE Iran: A transition between collision and subduction through a young deforming system. *Tectonics* 23, TC4007. https://doi.org/10.1029/2003TC001599

Ritz J.F., Nazari H., Ghasemi A., Salamati R., Shafei A., Solaymani S. & Vernant P. 2006: Active transtension inside Central Alborz: A new insight into northern Iran–southern Caspian geodynamics. *Geology* 34, 477–480. https://doi.org/10.1130/G22319.1

Saberi E., Yassaghi A. & Djamour Y. 2017: Application of geodetic leveling data on recent fault activity in Central Alborz, Iran. *Geophysical Journal International* 211, 751–765. https://doi.org/10.1093/gji/ggx311

Saidi A. & Ghassemi M.R. 1991: Geological map of Baladeh Quadrangle Scale 1:100,000. *Geological Survey of Iran*.

Tatar M., Jackson J., Hatzfeld D. & Bergman E. 2007: The 2004 May 28 Baladeh earthquake (M_w 6.2) in the Alborz, Iran: overthrusting the South Caspian Basin margin, partitioning of oblique convergence and the seismic hazard of Tehran. *Geophysical Journal International* 170, 249–261. https://doi.org/10.1111/j.1365-246X.2007.03386.x

Vahdati-Daneshmand F. 2001: Geological map of Marzan Abad Quadrangle Scale 1:100,000. *Geological Survey of Iran*.

Vernant Ph., Nilforoushan F., Hatzfeld D., Abbassi M.R., Vigny C., Masson F., Nankali H., Martinod J., Ashtiani A., Bayer R., Tavakoli F. & Chéry J. 2004: Present-day crustal deformation and plate kinematics in the Middle East constrained by GPS measurements in Iran and northern Oman. *Geophysical Journal International* 157, 381–398. https://doi.org/10.1111/j.1365-246X.2004.02222.x

Yamaji A., Sato K. & Otsubo M. 2011a: Multiple Inverse method Software Package, mim60, Version 6.2 and miv4, Version 4.17. *Division of Earth & Planetary Sciences Kyoto University*.

Yamaji A., Sato K. & Otsubo M. 2011b: Multiple Inverse method Software Package, User's Guide. *Division. Division of Earth & Planetary Sciences Kyoto University*.

Yassaghi A. 2001: Inversion tectonics in the Central Alborz Range. In: *European Union of Geosciences (EUG XI). Symposium LS05*, Abstract, 335.

Yassaghi A. & Madanipour S. 2008: Influence of a transverse basement fault on along-strike variations in the geometry of an inverted normal fault: Case study of the Mosha Fault, Central Alborz Range, Iran. *Journal of Structural Geology* 30, 1507–1519. https://doi.org/10.1016/j.jsg.2008.08.006

Yassaghi A. & Naeimi A. 2011: Structural analysis of the Gachsar sub-zone in Central Alborz range; constrain for inversion tectonics followed by the range transverse faulting. *Earth Sciences* 100, 1237–1249. https://doi.org/10.1007/s00531-010-0537-y

Yousefi E. & Friedberg J.L. 1977: Aeromagnetic map of Iran (Amol). Scale 1: 250,000. Geological survey of Iran, Tehran.

Zamani G.B. & Masson F. 2013: Recent Tectonics of East (Iranian) Azerbaijan from stress state reconstructions. *Tectonophysics* 611, 61–82. https://doi.org/10.1016/j.tecto.2013.10.015

Zanchi A., Berra F., Mattei M., Ghassemi M.R. & Sabouri J. 2006: Inversion tectonics in central Alborz, Iran. *Journal of Structural Geology* 28, 2023–2037. https://doi.org/10.1016/j.jsg.2006.06.020